FULL PAPER

Osteogenic/Angiogenic Dual Growth Factor Delivery Microcapsules for Regeneration of Vascularized Bone Tissue

Ramesh Subbiah, Mintai Peter Hwang, Se Young Van, Sun Hee Do, Hansoo Park, Kangwon Lee, Sang Heon Kim, Kyusik Yun, and Kwideok Park*

Growth factors (GFs) are major biochemical cues for tissue regeneration. Herein, a novel dual GF delivery system is designed composed of poly(lactic-*co*-glycolic acid) (PLGA) nanoparticles (NPs) and alginate microcapsules (MCs) via an electrodropping method. While bone morphogenetic protein (BMP)-2 is encapsulated in the PLGA NPs, vascular endothelial growth factor (VEGF) is included in the alginate MCs, where BMP-2-loaded PLGA NPs are entrapped together in the fabrication process. The initial loading efficiencies of BMP-2 and VEGF are 78% ± 3.6% and 43% ± 1.7%, respectively. When our dual GF-loaded MCs are assessed for in vitro osteogenesis of umbilical cord blood-derived mesenchymal stem cells (UCB-MSCs) on 2D and 3D environment, MCs contribute to much better UCB-MSCs osteogenesis as confirmed by von Kossa staining, immunofluorescence (osteocalcin, collagen 1), calcium content measurement, and osteogenic markers expression. In addition, when dual GF-encapsulated MCs are combined with collagen and then applied to 8 mm diameter rat calvarial defect model, the positive effects on vascularized bone regeneration are much more pronounced; micro computed tomography (CT) and histology analyses exhibit 82.3% bone healing coupled with 12.6% vessel occupied area. Put together, current study indicates a synergistic effect of BMP-2/VEGF and highlights the great potential of dual GF delivery modality (PLGA NPs-in-MC) for regeneration of vascularized bone.

1. Introduction

Vascularized bone tissue regeneration for the treatment of various bone defects still remains extremely challenging.[1] Therapies using genes,[2] stem cells,[3] and growth factors (GFs)[1,4] are major strategies employed by researchers to induce vascularization during new bone formation and to overcome some drawbacks associated with conventional treatment modalities, such as the use of autografts, allografts, and xenografts. Since a report of dual GF-mediated angiogenesis by Richardson et al.,[5] several groups have examined the effect of dual GF delivery on the regeneration of complex tissues such as angiogenesis,[6] chondrogenesis,[7] myogenesis,[8] osteogenesis,[9–15] and neurogenesis.[4] In particular, studies regarding dual GF-mediated osteogenesis have yet to provide any conclusive findings; while several works reported on an augmented level of osteogenesis via dual GFs delivery,[12–15] others reported on an insignificant level of osteogenesis.[16–18] For instance, Kanczler et al. demonstrated the interplay of osteogenic (bone morphogenetic protein-2; BMP-2) and angiogenic GFs (vascular endothelial GF; VEGF) brings augmented bone formation than that achieved by BMP-2 alone.[13] Similarly, Patel et al. found enhanced bone bridging and union but no significant difference on bone formation by BMP-2 and VEGF than by BMP-2 alone in rat cranial defect.[17] In addition, Kempen et al. reported combination of BMP-2 and VEGF produces synergistic effect on ectopic bone formation but not on orthotopic bone formation.[19] Hence it is widely recognized that selection of appropriate GFs, doses, and delivery system is a very important strategy in achieving

R. Subbiah, M. P. Hwang, S. Y. Van, Prof. K. Lee, Prof. S. H. Kim, Prof. K. Park
Center for Biomaterials
Korea Institute of Science and Technology (KIST)
Seoul 136-791, South Korea
E-mail: kpark@kist.re.kr
R. Subbiah, S. Y. Van, Prof. K. Lee, Prof. S. H. Kim, Prof. K. Park
Department of Biomedical Engineering
Korea University of Science and Technology (UST)
Daejon 305-333, South Korea

Prof. S. H. Do
Department of Veterinary Clinical Pathology
Konkuk University
Seoul 143-701, South Korea
Prof. H. Park
School of Integrative Engineering
Chung-Ang University
Seoul 156-756, South Korea
Prof. K. Yun
College of Bionanotechnology
Gachon University
Seongnam 461-701, South Korea

successful regeneration of vascularized bone tissue. However, the rationale behind such combination of specific GFs and carrier system is still unclear and poorly defined in many instances, due mainly to the complexity of biological functions of GFs in vivo and difficulty in controlling GFs release rate.

Since many investigations have alleged some controversial effects of single or dual GFs delivery on osteogenesis and/or bone healing, this study intends to systemically investigate the benefits of sustained in situ delivery of dual GFs for osteogenesis of umbilical cord blood-derived mesenchymal stem cells (UCB-MSCs) in a 2D and 3D culture environment and more importantly for a vascularized new bone formation via a rat calvarial bone defect model. To do this, we design and prepare a dual GF carrier system for sustained delivery of BMP-2 and VEGF. There are many candidates in fabricating drug delivery systems, including synthetic polymers, biopolymers, and inorganic compounds. Among them, we choose alginate and poly(lactic-co-glycolic acid) (PLGA) for their proven efficacy and versatile advantages.[6,20–22] Alginate is very useful and easy to handle for encapsulation of bioactive molecules, cells, or micro/nanoparticles. PLGA is a biodegradable polymer and very flexible in fabricating micro/nanoparticles. Our dual GF delivery platform is composed of alginate microcapsules (MCs), which include PLGA nanoparticles (NPs); BMP-2 is encapsulated in the PLGA NPs and VEGF is entrapped into the alginate matrix. Our electrodropping system has been very useful in producing uniform sized MCs. The set up of the electrodropping apparatus is simple that allows continuous and automated production of MCs. In addition, this technique offers high production yield, increased encapsulation efficiency, and minimal aggregation of MCs.[23–25] Among the previous works, there are few equivalents to our platform in which a dual GF(VEGF/BMP-2) delivery system was fabricated via electrodropping method. The combined use of dual GF delivery system and UCB-MSCs for vascularized bone regeneration is also notable in this work, due to the clinical applications of UCB-MSCs in stem cell therapy.

We hypothesize that in situ delivery of dual GFs should have an added or synergistic effect on the osteogenic differentiation of UCB-MSCs in vitro and more importantly on vascularized new bone formation when delivered in vivo. In general, VEGF and BMP-2 are considered to be a common and potent combination for vascularized bone tissue regeneration. Previous report manifests VEGF secretion happened at the earlier healing stage of bone fracture, whereas BMP-2 secretion during entire fracture healing process.[26] To this end, it would be very interesting to see the results that compared to single GF (BMP-2)-loaded MCs, dual GF-loaded MCs could significantly enhance calvarial bone regeneration at the interfacial area between host and transplant as well as in the bulk defect region, along with a notable volume of vascularization. This study clearly indicated a synergistic impact of two different GFs on the regeneration of vascularized bone tissue and demonstrated the role of carrier system that enables sustained delivery of dual GFs from MCs at the target site.

2. Results and Discussion

2.1. Preparation and Characterization of MCs

A GF delivery system of core–shell MCs was proposed in the previous study.[6] However, fabrication of homogeneous core–shell MCs using electrodropping method depends on various parameters including physicochemical properties of polymers, coaxial needle set up, electrostatic repulsion, and flow rate.[10] Herein, a new MC design is attempted via PLGA NPs and alginate for dual GF delivery. BMP-2-loaded PLGA NPs are produced (**Figure 1**A) by employing an ultrasonication-assisted double emulsion evaporation method.[27] The size and surface charge of the PLGA NPs were found to be 138 ± 53 nm and −18 ± 0.9 mV, respectively. Scanning electron microscope (SEM) and atomic force microscope (AFM) images of PLGA NPs showed a homogeneous
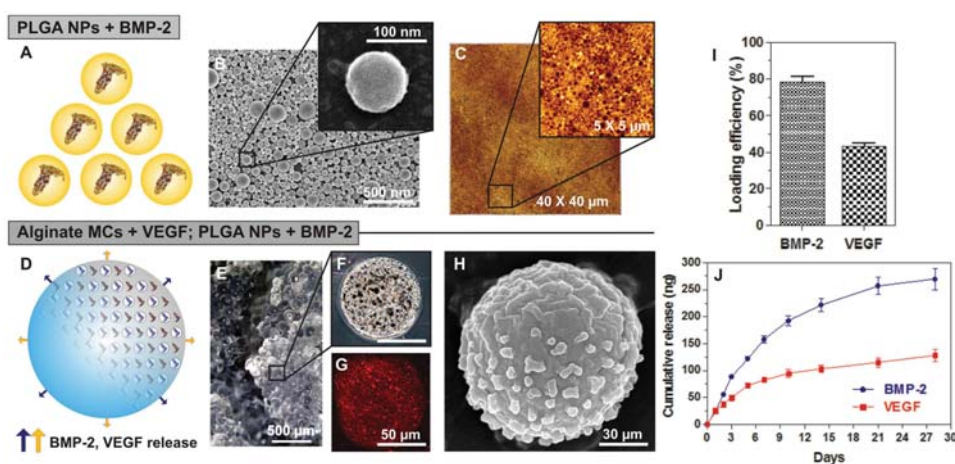

Figure 1. Dual GF-loaded microcapsules (MCs) fabrication and characterization. A) BMP-2-loaded PLGA NPs exhibit a fairly homogenous distribution of spherical particles, as assessed via B) SEM and C) AFM. D) BMP-2-loaded PLGA NPs and VEGF are encapsulated into alginate to generate dual GF-loaded MCs for the sequential release of GFs (arrows). E) The dual GF-loaded MCs are examined via gross appearance and F) optical microscopy, which indicate the presence of PLGA NPs (black spots). G) Fluorescence of rhodamine red-stained PLGA NPs in the MC and H) SEM image of MC. I) The initial loading efficiency of BMP-2 and VEGF, respectively and J) the release profile of two different growth factors out of the dual GF-loaded MCs as observed for 28 d in vitro.

ADVANCED
HEALTHCARE
MATERIALS
www.advhealthmat.de

Materials
Views
www.MaterialsViews.com

FULL PAPER

distribution of spherical particles (Figure 1B,C). Their surface roughness was 29 ± 3.5 nm. The synthesized PLGA NPs were then encapsulated into alginate MCs to carry out sustained delivery of dual GFs. Alginate was chosen due to its versatile use as a delivery carrier material for multiple factors (e.g., cells and proteins),[21] and for its simple cross-linking mechanism via divalent cation solutions. An electrodropping technique was employed to fabricate dual GF-loaded MCs: BMP-2-loaded PLGA NPs and VEGF-encapsulated alginate (Figure 1D). Loading BMP-2 in PLGA NPs may provide a separate domain to store GF and to avoid a random interaction between GFs in MCs. The size and morphology of the MCs can be controlled via varying the concentration of alginate solution, syringe flow rate, and applied electric field.[10] Using an alginate solution (1%, w/v) with a 120 µL min^{-1} flow rate and 11 kV, the size and surface charge of the MCs were determined to be 105 ± 12 µm and −23.5 ± 1.2 mV, respectively. The soft MCs (E = 7.4 ± 0.8 kPa) maintain a spherical morphology (Figure 1E,F) and the PLGA NPs are homogenously distributed within the MCs, visually confirmed via the use of rhodamine-encapsulated PLGA NPs (Figure 1G). A magnified SEM image showed a slightly crinkled alginate surface with some protrusions (Figure 1H). It seems that the protrusions happened to result from the dispersed PLGA NPs, during encapsulation into alginate. The loading efficiency of GFs after fabrication of MCs was examined using enzyme-linked immunosorbent assay (ELISA). Beginning with 500 ng of each GF, the initial loading efficiency of BMP-2 in PLGA NPs and VEGF in alginate was 78% ± 3.6% (392 ± 18 ng) and 43% ± 1.7% (216.5 ± 8.8 ng), respectively (Figure 1I).

In addition, the resulting dual GF-loaded MCs were investigated for GF release kinetics via a transwell system. The release profiles demonstrate the independent GFs release kinetics. The release efficiency of BMP-2 and VEGF from the MCs in a given time period (28 d) was found to be 69% ± 5% (270 ± 20 ng) and 59% ± 5% (128 ± 11 ng), respectively (Figure 1J). Early burst release of ≈23% BMP-2 (88 ng) and ≈23% of VEGF (37 ng) was observed during first 3 d, followed by ≈34% of BMP-2 (134 ng) and 25% of VEGF (25 ng) release between day 4 to 14. Overall, the MCs continued the release of both GFs for up to 28 d and exhibited a different release kinetics, in which BMP-2 was released at a higher concentration than VEGF. It should be addressed at this point that both loading efficiency and release profile are indirect evidences regarding BMP-2 bioactivity when delivered from PLGA NPs. Direct evidences can be obtained from in vitro and in vivo experiments. The following results suggest that current fabrication process of MCs is acceptable, not significantly hamper the bioactivity of BMP-2. In fact, polymer NPs and MCs have been widely utilized as a delivery carrier of GF, protein, peptide, and drugs and for tissue engineering applications.[22,28,29] It is generally accepted that NPs and MCs not only increase the stability of loaded GFs but prolong the half-life of GFs. In addition, they can be integrated with a transplantable 3D scaffold for targeted tissue regeneration.

2.2. Induction of 2D Osteogenesis

The effect of single or dual GF release from the MCs on the induction of 2D osteogenic differentiation of UCB-MSCs was evaluated using four different groups (**Figure 2**A). The level of osteogenesis was examined after 14 and 28 d of osteogenic induction in vitro, respectively. All four groups showed positive black stains of mineralized area as assessed via von Kossa staining at 28 d (Figure 2B); quantification of the area positively stained was 66.5% ± 6% (G1), 80% ± 6% (G2), 71.6% ± 7% (G3), and 81% ± 7% (G4) (Figure 2G). Immunofluorescence staining (IFS) results (Figure 2D,E) of osteogenic protein markers, osteocalcin (OCN), and collagen type 1 (Col 1) yield similar results as that of von Kossa staining. Figure 2F shows a merged image of 4′,6-diamidino-2-phenylindole (DAPI; Figure 2C), and IFS of OCN and Col 1. Quantitative analysis of OCN (Figure 2H) and Col 1 (Figure 2I) fluorescence indicates the following order of osteogenic efficiency: G4 ≥ G2 > G3 > G1. In particular, positive staining of OCN was significantly higher among the cells treated with dual GF-loaded MCs (G4) than those incubated with a single GF (G3) (Figure 2H). Additionally, when each group was assessed for osteogenic gene expression, bone sialoprotein (BSP), Col 1, OCN, and osteopontin (OPN) were significantly overexpressed in groups of G2, G3, and G4 compared to G1 (Figure 2J). While not much difference in expression level was observed among G2, G3, and G4, the one of BSP was higher in G4 than in G3. Also, the average expression levels of OPN, and Col 1, while not significant, were greater in G4 than that observed in the other groups. Each group was also assessed for osteogenesis via calcium content measurement (Figure 2K). As expected, the normalized calcium content for the groups supplied with GFs (G2, G3, and G4) was larger than that of G1. In addition when gene expression levels and calcium content were evaluated after 14 d of culture, the outcomes were similar with those observed at 28 d (Supporting Information, Figure S1). Overall, the results of 2D osteogenesis prove that our MCs sustainably release bioactive dual GFs for at least 28 d to promote osteogenesis of UCB-MSCs on 2D culture. It should be noted that the cumulative BMP-2 release from current MCs platform is approximately 270 ng BMP-2, a little over half of that supplied exogenously via medium for G2 (500 ng). The present results coincide with the report of Zhang et al., where they demonstrated the synergistic osteogenic response of adipose-derived stem cells (ADSC) via dose-dependent VEGF and BMP-6 combined delivery than via VEGF or BMP-6 delivery alone.[30] They claimed the synergistic effect was due to a cross talk between VEGF and BMP signaling pathway for the enhancement of osteogenesis.

2.3. Induction of 3D Osteogenesis

It is well known that 2D cell culture does not take into account the complexity of biological, physical, and mechanical properties of natural cellular microenvironment. Hence, we have fabricated a 3D collagen scaffold disc (approximately 8 mm Ø and 2 mm thickness) encapsulating both UCB-MSCs and MCs (**Figure 3**A). Unlike 2D cell culture, collagen scaffold provides cells with an excellent extracellular microenvironment, wherein UCB-MSCs are able to proliferate, interact with the surroundings, and respond to the released dual GFs from MCs, in 3D. White spots inside the collagen scaffold depict the distribution of MCs (Figure 3B), and an interconnected fibrous network of
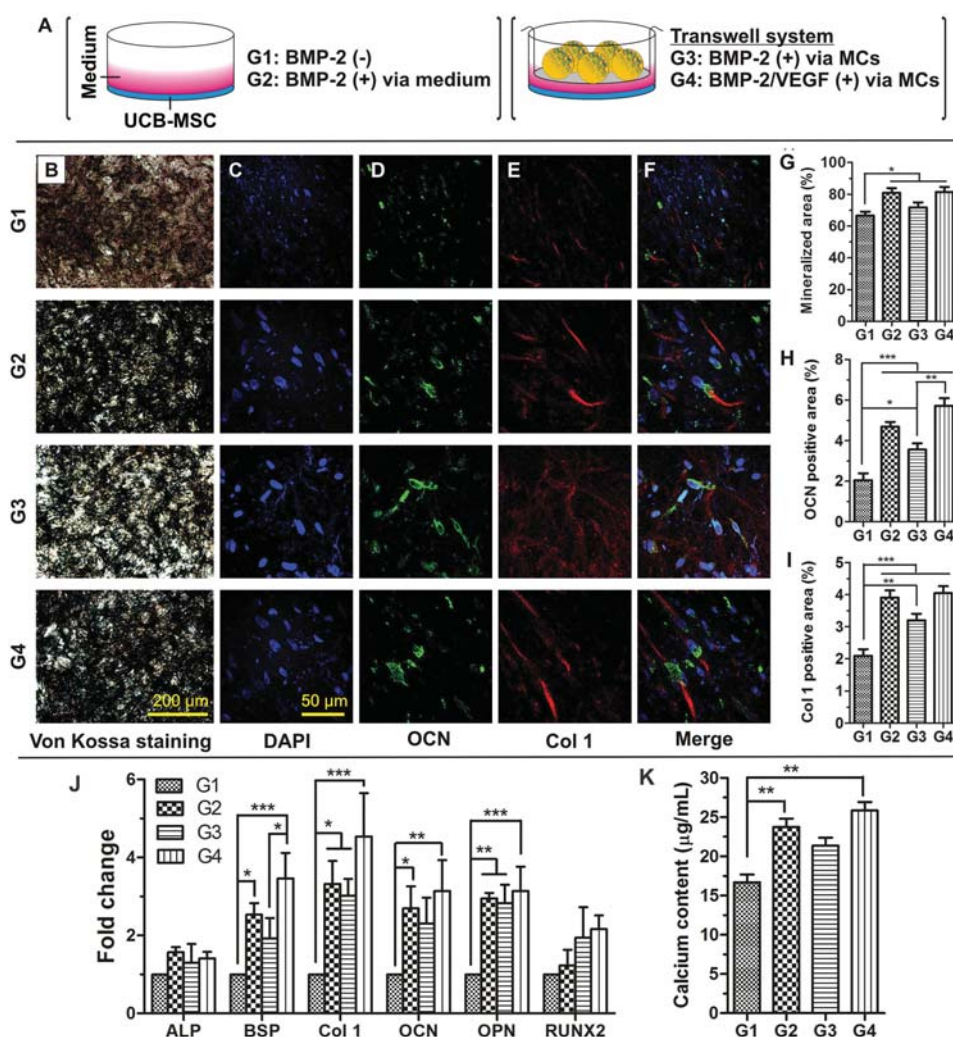
Figure 2. 2D osteogenic induction of UCB-MSCs. A) UCB-MSCs are seeded in six-well plates and cultured in one of four groups. After 28 d, cells are examined via B) von Kossa staining, C) DAPI staining (blue) for the nucleus, and IFS of D) osteocalcin (OCN, green), and E) collagen 1 (Col 1, red), F) merged images. Positively stained areas are quantified for G) mineralized area, H) OCN, and I) Col 1 images via image J software. J) qPCR of several osteogenic markers (ALP, BSP, Col 1, OCN, OPN, and RUNX2) indicate higher expression levels for all groups relative to G1. K) Normalized calcium content is much higher in G2 and G4 than that of G1. Results are mean ± standard deviation (SD) of triplicate measurements and are representative of three independent experiments. ***$p < 0.001$, **$p < 0.01$, and *$p < 0.05$ indicate a statistically significant difference, respectively.

the collagen is observed via AFM (Figure 3C). This collagen scaffold is supposed to provide 3D microenvironment for UCB-MSCs and to retain bioactivity of GFs within the scaffold. A cross-sectional SEM image clearly delineates MCs (depicted as stars) embedded in the collagen matrix (Figure 3D). Proper mixing at 4 °C was essential during scaffold fabrication to ensure the distribution of cells and MCs; PKH67 staining confirmed the presence of UCB-MSCs in the collagen scaffold (Figure 3E) and the broad distribution throughout the scaffold at the center (Figure 3F) and in the periphery (Figure 3G). The black cavities correspond to the MCs and the green spots correspond to PKH67-stained cells. As illustrated in **Figure 4**A the level of osteogenesis of UCB-MSCs in collagen scaffold was analyzed after 28 d of in vitro culture. Low and high magnification (Figure 4B) images of von Kossa stains confirmed the presence of mineralized area for all groups. Quantification

of the stained areas was measured to be 6.5% ± 0.6% (G1), 13.7% ± 0.8% (G2), 14.7% ± 0.9% (G3), and 17% ± 0.9% (G4) (Figure 4G). IFS results (Figure 4D,E) of osteogenic protein markers OCN and Col 1 yield a similar trend as that of von Kossa staining. Figure 4F shows a merged image of DAPI, and IFS of OCN and Col 1. Quantitatively compared, the order of osteogenic efficiency: G4 > G3 > G2 > G1 (Figure 4H,I). Additionally, when osteogenic gene expression was assessed by real-time quantitative polymerase chain reaction (qPCR; Figure 4J), all markers were significantly upregulated in G4 than in other groups. However, less osteogenic activity was observed from G2 compared to that of G3 or G4, due mainly to certain role of VEGF on osteogenesis[31] and poor diffusion of BMP-2 into the interior of the scaffold when provided exogenously.[32] While VEGF is a potent angiogenic inducer, it is reported to stimulate osteoblast differentiation and believed to support a
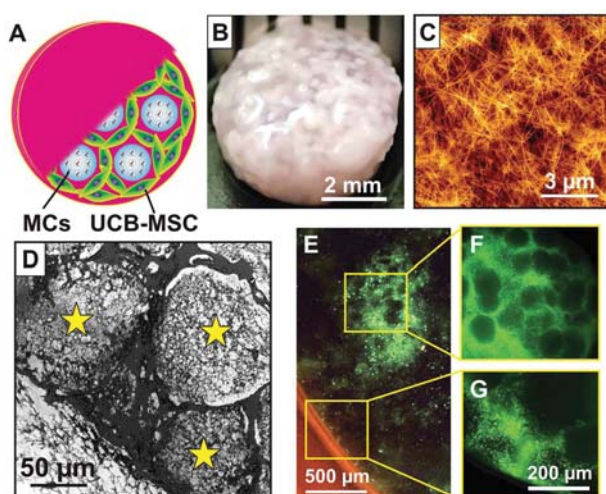
Figure 3. Characterization of collagen scaffolds containing UCB-MSCs and dual GF-loaded MCs. A) UCB-MSCs and dual GF-loaded MCs are prepared as a homogenous mixture and encapsulated in collagen matrix. B) Gross appearance of the resulting collagen scaffolds and C) AFM, in which the topography image shows a fibrous collagen structure. D) The cross-section of the collagen scaffolds is examined via SEM, and exhibits the presence of MCs (stars) within collagen matrix. E) PKH67-stained UCB-MSCs (green) are well distributed within the collagen scaffold as confirmed by fluorescence microscopy. In particular, the black cavities correspond to the MCs while the green spots correspond to PKH67-stained cells. F) Inner and G) peripheral region of collagen scaffold.

synergistic effect of osteogenesis along with BMP-2.[31] Each group was also assessed for calcium content (Figure 4K). The normalized calcium content was much higher in groups using MCs (G3 and G4) and the difference was statistically significant. Meanwhile, the results of gene expression and calcium content analyzed at 14 d were also similar to those at 28 d (Supporting Information, Figure S2). Weinand et al. reported that controlled delivery of BMP-2 via gelatin hydrogel microspheres within 3D scaffold promoted augmented osteogenesis of stem cells derived from human adipose (hASCs) and human bone marrow (hBMSCs).[33] The main interest was to compare the osteogenic potentials between hASCs and hBMSCs in vitro; the role of microspheres and its characterization were not properly addressed. Gabbay et al. exhibited a significant enhancement of osteogenic differentiation of ADSCs while cultured in 3D scaffold than that cultured in 2D monolayer.[34] Taken together, similarly to 2D osteogenesis, it is notable that better osteogenic responses observed in G4 than in G3, most likely due to the positive effect of dual GFs within the 3D scaffold.

2.4. Vascularized Bone Regeneration

After demonstration of dual GF effect on osteogenesis in vitro, we considered a critical size (8 mm) rat calvarial defect model to demonstrate the capacity of our dual GF-loaded MC system for the regeneration of vascularized bone tissue. Studies were carried out for 28 and 56 d, and the results were assessed via micro CT, IFS, SEM, and histology. Temperature-sensitive rat tail collagen was served as a scaffold with a diameter of 8 mm and a thickness of 1.5 mm. A composite disc of collagen and

dual GF-loaded MCs was successfully prepared in an implantable form (**Figure 5**A). The experimental groups were set as G1 (defect only), G2 (BMP-2 loaded into collagen), G3 (BMP-2 delivered from single GF-loaded MCs), and G4 (BMP-2/VEGF delivered from dual GF-loaded MCs) (Figure 5B). Images of the calvarial defect site as assessed via X-ray and micro CT indicate a significant difference of bone regeneration at 28 d (Supporting Information, Figure S3) and at 56 d postoperation (Figure 5C,D). In particular, qualitative bone formation in G4 was significantly better than that observed in G1, G2, and G3. G1 group remains mostly empty supporting that the 8 mm sized defect is critical and self-healing is impossible. Quantification of the data was determined as bone volume (mm³) and percentage of bone regeneration measured within a given region of interest (Figure 5E,F). A higher level of bone regeneration was observed when BMP-2 was delivered from MCs (G3) rather than from the collagen (G2), suggesting that BMP-2 released from MCs was bioactive and more effective in bone healing. More interestingly it was clear that G4 showed the highest levels of bone volume and regeneration, followed by G3, G2, and G1, in decreasing order (Figure 5E,F). This result strongly hints a synergistic effect of dual GFs that VEGF may play a certain role in promoting a bone healing process. In addition, bone regeneration by dual GF in MCs-loaded scaffold was also evaluated via von Kossa staining (**Figure 6**A); the most mineralized deposit was detected in G4, followed by G3, G2, and G1 as quantitatively determined (Figure 6D). The protein levels of osteogenesis were also examined via IFS for OCN and Col 1 (Figure 6B). While high magnification IFS images (Figure 6C) confirm the positive expression of OCN and Col 1 for all groups, quantification of the fluorescence signals demonstrates the following osteogenic trend: G4 > G3 > G2 > G1 (Figure 6E,F). Specifically, G4 yields ≈three and ≈six fold higher levels of OCN and Col 1 expression, respectively, than those of G1. G4 also displays much higher expression of OCN than G2 and G3. Taken together, these findings imply that the mode of GF delivery is crucial and impact of dual GFs is very positive on current calvarial bone healing. Given that the dual GF-loaded MCs (G4) promoted the highest level of bone regeneration, the role of VEGF on vascularized bone regeneration is a particular interest in this study because active vascular network is a prerequisite for successful functional bone regeneration. In fact, VEGF is a well-known angiogenic factor and plays an important role in angiogenesis within bony bridging to achieve vascularized bone regeneration.[1,26,31] VEGF not only actively participates in the development of the vascular system but exhibits significant role in skeletal growth. It is reported that VEGF secretion is initiated in the earlier healing stage right after bone damage. Therefore, primary interest is posted on the level of vascularization of our transplants in the calvarial defect models. The thin-sectioned samples were stained with H&E for histological analysis (**Figure 7**A–C). The H&E stains of sagittal section of entire calvarial bone appear in Figure 7A. High magnification images taken at the interface region (marked in blue arrows) between newly regenerated bone and host bone tissue are also obtained (Figure 7B). A significant difference at the interfacial bone healing was obvious; a nearly full integration between host tissue and transplants was notable only with G4 as assessed by tissue thickness and interconnectivity. Upon the
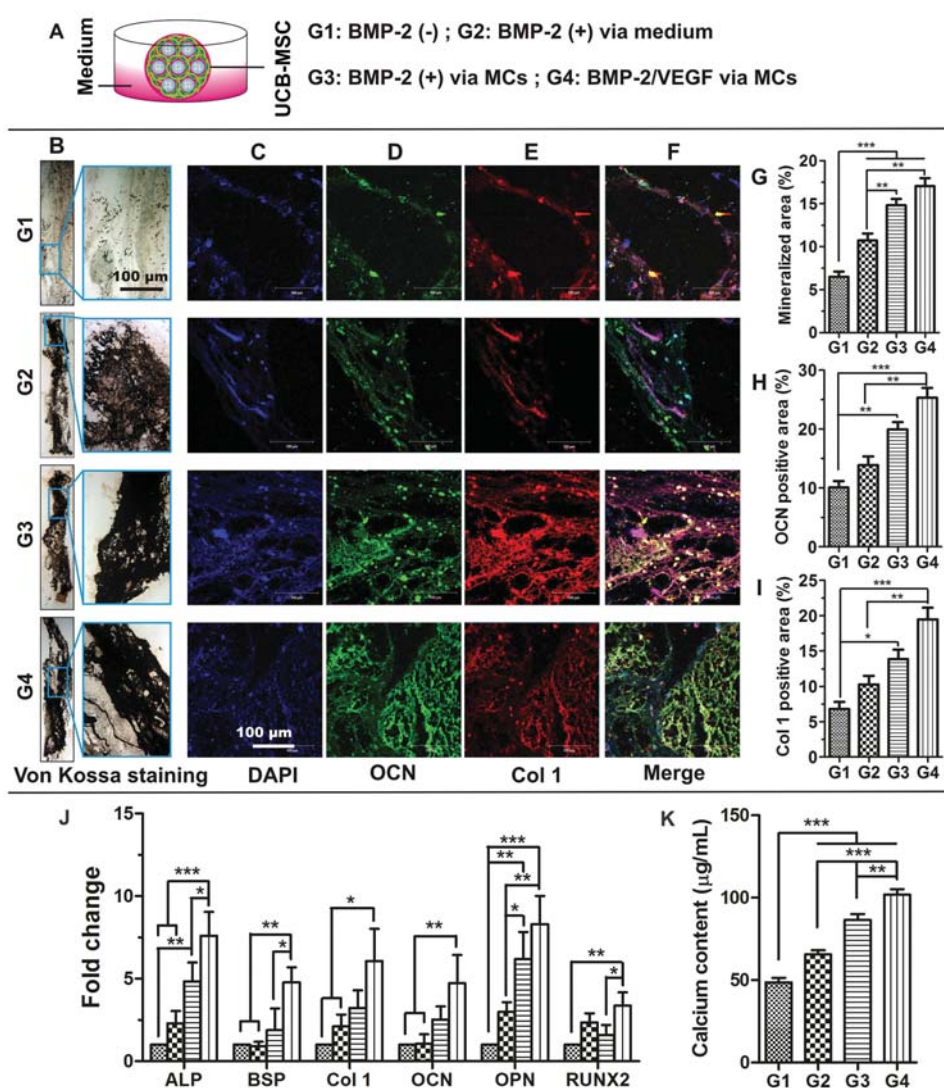
Materials
Views
www.MaterialsViews.com

ADVANCED
HEALTHCARE
MATERIALS
www.advhealthmat.de

FULL PAPER

Figure 4. 3D osteogenic induction of UCB-MSCs. A) UCB-MSCs (1×10^6) are encapsulated in the collagen scaffold and cultured in one of 4 groups. After 28 d, samples are vertically cross-sectioned and assessed via B) von Kossa staining at low and high magnification (extended box), C) DAPI staining (blue) for the nucleus, and IFS of D) osteocalcin (OCN, green), and E) collagen 1 (Col 1, red), F) merged images. Positively stained areas are quantified for G) mineralized area, H) OCN, and I) Col 1 images via image J software. J) qPCR of several osteogenic markers presents significantly higher expression levels in G4 than in G1, G2, and G3. K) Normalized calcium content is also much larger in G4 than that of the other three groups and the difference is statistically significant. Results are mean ± SD of triplicate measurements and are representative of three independent experiments. ***$p < 0.001$, **$p < 0.01$, and *$p < 0.05$ indicate a statistically significant difference, respectively.

examination of cell penetration into the transplants, it seems that cells migrated and mostly localized in the upper side of the transplant, forming a rich vasculature in the bony bridges (Figure 7C).

Interestingly this phenomenon was not as pronounced in G1, G2, and G3. Dual GFs may consequently stimulate cell migration (chemotaxis) toward the transplants from the surrounding tissues and cell populations are much dense in G4. It is unclear at this time about which GF is more responsible for cell migration. Previous studies have suggested a dose-dependent chemoattractive effect of VEGF on primary human osteoblasts, human mesenchymal progenitor cells, and osteoclasts.[31] Quantification of vessel density and vessel occupied area indicates that

G4 has approximately three- to four-fold higher levels than those of G3, G2, and G1 (Figure 7D,E). In addition, when mature blood vessel markers von Willebrand factor (vWF) and α-smooth muscle actin (α-SMA) was examined via IFS (**Figure 8**A), the highest level of vWF and α-SMA expression was noticed in G4 as quantitatively assessed (Figure 8E,F), followed by G2, G3, and G1, in decreasing order. SEM was also used to further analyze the development of new vessels; Figure 8B exhibits a whole cross-sectional view of each group. Figure 8C,D shows the SEM images of peripheral and inner region of the sections, respectively. The presence of red blood cells (RBCs) (marked as red arrows; blue triangles and lines indicate the upper boundary area of each sample) was confirmed in all groups. In particular,
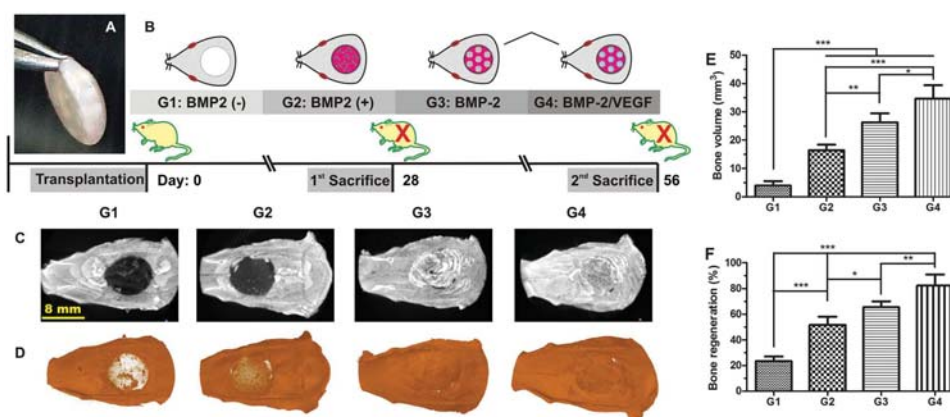
ADVANCED
HEALTHCARE
MATERIALS
www.advhealthmat.de

Materials
Views
www.MaterialsViews.com

FULL PAPER

Figure 5. Application of dual GF-loaded MCs for rat calvarial bone defect model. 8 mm size calvarial defects are created in seven week-old SD rats. A) collagen scaffolds containing dual GF-loaded MCs are prepared. B) Rats are divided into four groups and sacrificed at 28 and 56 d, respectively. Rat calvarium samples harvested at 56 d post-surgery are analyzed via C) X-ray and D) reconstructed micro CT images of regenerated bone defects. E) Bone volume in the calvarial defect region is quantified using CTan-3D analyzer. F) Bone regeneration percentage is quantified using an 8 mm ROI in the calvarial defect region. Results are mean ± SD and representative of 4 independent experiments. ***$p < 0.001$, **$p < 0.01$, and *$p < 0.05$ indicate a statistically significant difference, respectively.

new blood vessels, found in the peripheral regions, were the most rich in G4 (Figure 8C). Furthermore, the amount of blood vessels observed around the MC was highest in G4, possibly due to the VEGF released from the MCs. Overall, on average 82.3% of bone healing (Figure 5F) and 12.6% of vessel occupied area (Figure 7E) was accomplished via the use of dual GF-loaded MCs (G4). The present calvarial data strongly demonstrate the positive effect of dual GFs on vascularized bone healing. We speculate that VEGF and BMP-2 may work in tandem to initiate and develop a vascularized new bone tissue. It should be however noted that this study is insufficient in delivering a mechanistic insight of dual GF delivery system on vascularized bone regeneration. It is thus highly recommended that further study need to focus more on mechanistic point of view.

3. Conclusions

This study is supposed to address the effect of our unique dual GF delivery system on osteogenesis of UCB-MSCs in vitro and vascularized bone regeneration in vivo. Alginate MCs containing VEGF and BMP-2 loaded PLGA NPs were successfully fabricated in a well-controlled manner. Tested in four different groups, it was interesting that the positive effect of dual GFs delivery on in vitro osteogenesis of UCB-MSCs was more pronounced in 3D environment, rather than in 2D, as confirmed via von Kossa staining, IFS, osteogenic markers expression, and calcium content measurements. In addition, using rat calvarial bone defect model, micro CT images, histology, and IFS revealed a significant improvement of neovascularization as
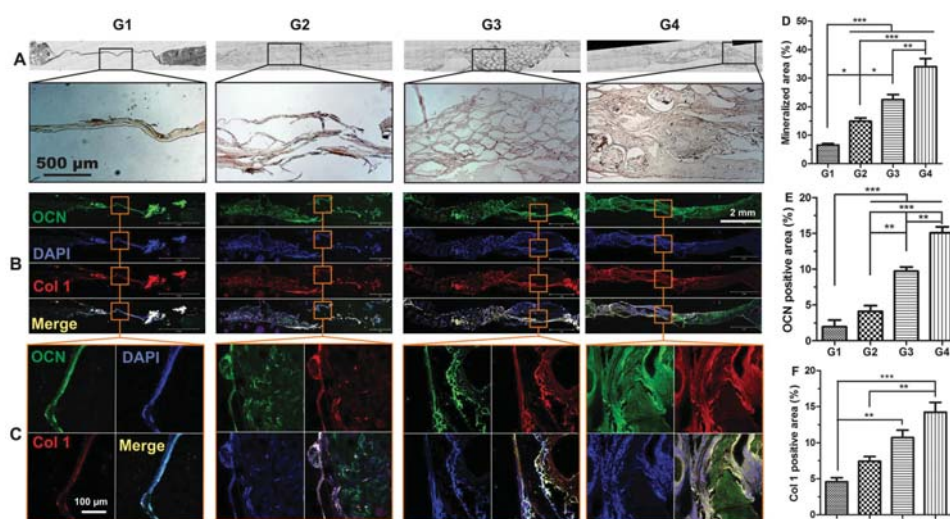

Figure 6. Histology and IFS of regenerated bone in a calvarial defect model. A) Rat calvarium samples are processed via von Kossa staining, B) DAPI staining (blue) for the nucleus, IFS of osteocalcin (OCN, green), and collagen 1 (Col 1, red). C) Higher magnifications of IFS images indicate much greater expression of OCN and Col 1 in G4 than in any other groups. Positively stained areas are quantified for D) mineralized area, E) OCN, and F) Col 1 images via image J software. Results are mean ± SD of triplicate measurements and are representative of three independent experiments. ***$p < 0.001$, **$p < 0.01$, and *$p < 0.05$ indicate a statistically significant difference, respectively.
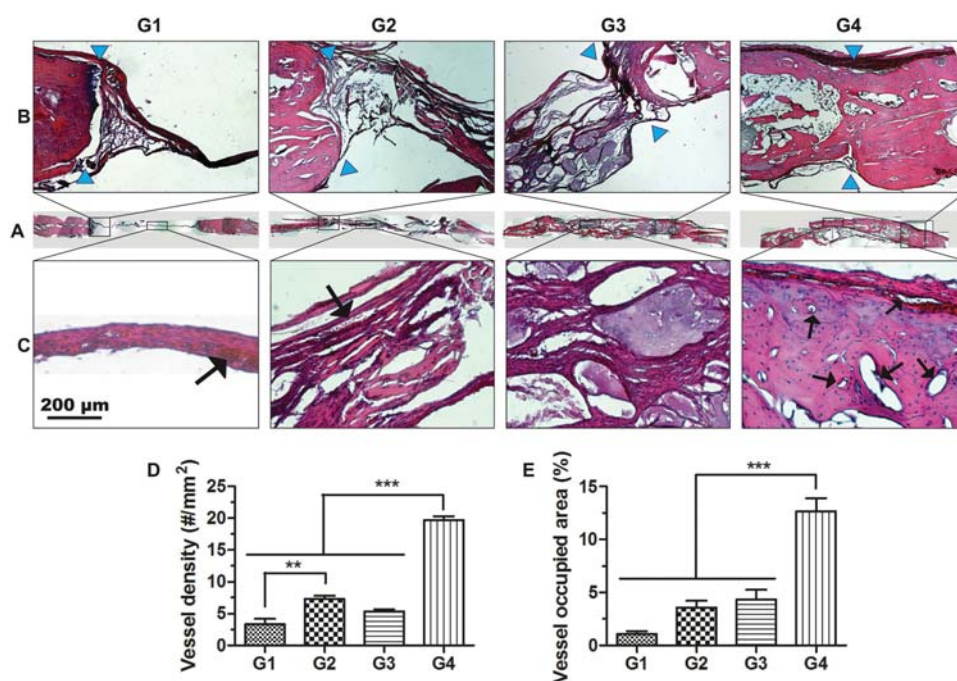
Figure 7. Histology (H&E staining) of the newly formed bone in a calvarial defect model. Rat calvarium samples are examined via low and higher magnifications of H&E stained images. The whole defect region of the calvarium is shown in A). While the interface region between the host bone and newly regenerated bone is marked in blue arrows B), the newly formed bone in the defect region is shown in C). Black arrows indicate red blood cells detected in a vascular structure. In addition, D) microvessel density and E) vessel occupied area within the defect site are also quantified using the histological images. Results are mean ± SD of triplicate measurements and are representative of three independent experiments. ***$p < 0.001$ and **$p < 0.01$ indicate a statistically significant difference, respectively.
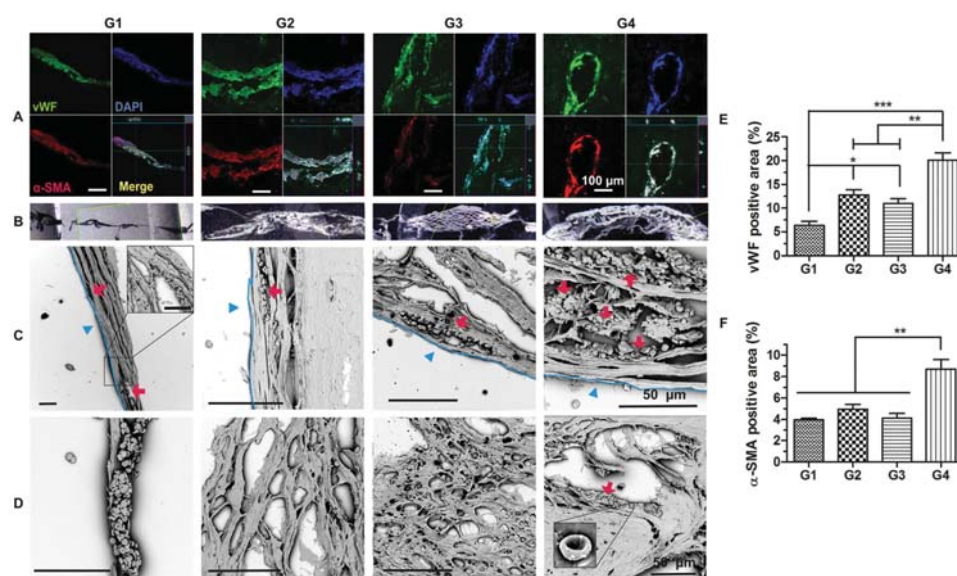

Figure 8. Vascularization in the newly formed bone for a calvarial defect model. Rat calvarium samples are examined via A) DAPI staining (blue) for the nucleus, IFS of von Willebrand factor (vWF, green), and α-smooth muscle actin (α-SMA, red). The regenerated defect sites are also analyzed via B) low magnification SEM images and higher ones for the C) peripheral and D) inner defect regions. Red arrows indicate red blood cells within a vascularized region (scale bar: 50 μm). The blue triangles and lines suggest the upper boundary area of each sample. Positively stained areas are quantified for E) vWF and F) α-SMA, respectively. Results are mean ± SD of triplicate measurements and are representative of three independent experiments. ***$p < 0.001$, **$p < 0.01$, and *$p < 0.05$ indicate a statistically significant difference, respectively.

**ADVANCED
HEALTHCARE
MATERIALS**

www.advhealthmat.de

*Materials
Views*

www.MaterialsViews.com

FULL PAPER

well as bone healing after 56 d postoperation; 82.3% of bone healing and 12.6% of vessel occupied area were noticed when treated only with dual GF-loaded MCs. Taken together, this study demonstrates that our dual GFs (VEGF and BMP-2) platform via PLGA NPs-in-MCs is a very effective delivery modality in promoting a synergistic effect on the regeneration of vascularized bone tissue.

4. Experimental Section

Dual GF-Loaded MC Fabrication: PLGA NPs were loaded with 500 ng of BMP-2 (R&D System; Minneapolis, MN) in 1% bovine serum albumin (BSA) using a modified protocol.[27] Briefly, PLGA NPs were prepared via an ultrasonication-assisted double emulsion evaporation method (Sonic Dismembrator Model 500, Fisher Scientific) using an oil phase of 6% w/v PLGA (75:25, RG 757S, MW: 270 000; Boehringer Ingelheim, Germany) and an aqueous phase of 5% w/v polyvinyl alcohol (PVA; 87%–89% hydrolyzed, MW 13,000–23,000; Aldrich). Simultaneously, 500 ng of VEGF (R&D System; Minneapolis, MN) in 1% BSA was added into a 1:1 (v/v) mixture of aqueous sodium alginate (1% w/v; 300–400 cp; Wako Chemicals, Osaka, Japan) and ethylene glycol (Sigma-Aldrich, St. Louis, MO). The PLGA NPs and alginate solution were then mixed thoroughly prior to MC fabrication. An electrodropping system (NanoNC, eS-robot electrospinning spray system, Seoul, Korea) was used under the following settings to prepare the dual GF-loaded MCs: 28G needle gauge, 120 µL min^{-1} flow rate, 11 kV applied electric voltage, and 10 cm distance between the nozzle tip and grounded collector (Supporting Information, Figure S4). The electrodropped MCs were immediately solidified in 1% w/v CaCl$_2$ solution, sequentially washed in 2.5% w/v PVA solution and deionized water (DW), filtered through a custom made vacuum assisted filtration set up using 8 µm pore size cell culture insert (Becton Dickinson Labware, 35–3182, France), and stored at 4 °C for future use.

Characterization: A PLGA NP emulsion was spin-coated onto a freshly cleaved mica substrate while stored MCs were placed on a glass substrate and dried in vacuum oven at 37 °C. Subsequently, field emission scanning electron microscopy (FE-SEM; Jeol 7500F, USA) and bio-AFM (Nanowizard II, JPK Instruments, Berlin, Germany) equipped with a HYDRA2R-50NG AFM probe (AppNano) were utilized to obtain morphological images of the particles. The average size and distribution of the particles were analyzed using a laser diffraction particle sizer (Malvern Mastersizer 2000, Malvern, UK). Rhodamine red-stained PLGA NPs were encapsulated in MCs to evaluate the distribution pattern of PLGA NPs inside alginate MCs. Finally, root mean square roughness (R_q) and stiffness (E, Young's modulus) of the MCs were analyzed using a BioAFM-based microindentation method, following a previous report.[35,36] The total amount of BMP-2 and VEGF loaded into the PLGA NPs and alginate MCs, respectively, was measured using an enzyme-linked immunosorbent assay (ELISA; R&D Systems). The CaCl$_2$ solution after MC solidification was collected and tested for determination of the loss of GFs. The initial loading efficiency (%) was calculated, based on the ratio between initial content of GF and lost amount of GF. To assess GF release, once dual GF-loaded MCs were put into 8 µm pore size Falcon cell culture inserts (Becton–Dickinson Labware; 35–3182), those inserts were placed inside 12-well culture plates containing predetermined volume of DW, and incubated at 37 °C for 28 d. DW samples were collected at specific time points, then replenished with fresh DW. The release efficiency (%) was also determined, based on the ratio between MC-loaded GF content and released amount of GF.

Preparation and Characterization of Collagen Scaffold Encapsulated with MCs and UCB-MSCs: Type I collagen, extracted from rat tail following a standard protocol,[37] was prepared in acetic acid, diluted with 1×, 10× Medium-199 (Lonza) and neutralized with 1 M NaOH. GF-loaded MCs were homogeneously mixed with 0.3% (w/v) collagen solution, followed by addition of UCB-MSCs (1 × 10^6) prestained with cell tracker dye PKH-67 (Sigma, USA). A disposable three-way stopcock (HS-T-01,

Hyupsung Medical Co., Ltd, Korea) was employed to thoroughly mix the MCs and UCB-MSCs with collagen. The entire procedure (Supporting Information, Figure S5) was carried out in an ice bath to prevent the gelation of collagen. The mixture was placed in the mold and allowed for gelation under a standard culture condition (37 °C, 5% CO$_2$) for 30 min, subsequently cultured in minimum essential medium alpha (α-MEM) supplemented with 10% fetal bovine serum (FBS) and 1% penicillin/streptomycin (P/S; Gibco BRL, Grand Island, MD). The distribution and viability of the PKH67-stained cells were imaged using fluorescence microscopy (CKX41-F32FL; Olympus, Japan). A composite collagen scaffold was photographed using a digital camera (TG-2; Olympus, Japan). Finally, SEM (Phenom G2 pro desktop, Eindhoven, Netherlands) images of the scaffold were obtained by fixing with 4% paraformaldehyde, dehydrating through a graded series of ethanol, embedding in paraffin, and sectioning into 5 µm thick slices. They were then sputter-coated with platinum, and photographed via SEM.

Induction of 2D Osteogenesis In Vitro: UCB-MSCs (passage 8–10) were seeded at a density of 2.5 × 10^4 cells cm^{-2} and cultured in α-MEM supplemented with 10% FBS and 1% P/S. To investigate the osteogenic potential of MCs in vitro, 50 mg of MCs in 8 µm pore size Falcon inserts were placed on six-well plates containing UCB-MSCs and cultured in osteogenic medium – α-MEM supplemented with 10% FBS, 1% P/S, 10 × 10^{-3} M β-glycerophosphate, 0.1 × 10^{-6} M dexamethasone, and 50 µg mL^{-1} L-ascorbic-2-phosphate – under standard culture conditions (37 °C and 5% CO$_2$). The experimental groups were set as G1 (without BMP-2), G2 (50 ng BMP-2 added exogenously in every medium exchange that accounts for 500 ng during 28 d), G3 (≈270 ng BMP-2 delivered from single GF-loaded MCs), and G4 (≈270 ng BMP-2/≈128 ng VEGF delivered from dual GF-loaded MCs). The medium was changed every 2 d and the UCB-MSCs were incubated for either 14 or 28 d. At the end of each time point, the samples were washed with phosphate buffered saline (PBS), fixed in 4% ρ-formaldehyde, and stored for subsequent osteogenic analysis.

Induction of 3D Osteogenesis In Vitro: A mixture of collagen, UCB-MSCs, and MCs with or without GFs were prepared as previously stated. The same initial loading amount of GFs as used on 2D was also applied. The collagen scaffolds were incubated in osteogenic medium for either 14 or 28 d under standard culture conditions (37 °C and 5% CO$_2$), and the medium was changed every 2 d. At the end of each time point, the scaffolds were retrieved, washed with PBS, fixed in 4% ρ-formaldehyde, dehydrated through a graded series of ethanol, embedded in paraffin, serially sectioned into 5 µm thick sections, and stored for subsequent osteogenic analysis.

Measurement of Calcium Content and Total Protein Amount: Calcium content and total protein amount are determined after 14 and 28 d to assess the osteogenic potential of MCs. 2D UCB-MSC cultures were treated with 0.5% Triton X-100 solution, scraped, collected, and vortexed for 30 min. Meanwhile 3D collagen scaffolds were added with 0.5% Triton X-100 solution and ultrasonicated using a probe tip sonicator for 10 min for scaffold homogenization. Calcium content and total protein amount were then measured using a QuantiChrom Calcium Assay Kit (DICA-500, BioAssay systems, USA) and a bicinchoninic acid (BCA) assay kit (Pierce), respectively, following the manufacturer's instructions. Samples were measured for their absorbance using a micro plate reader (Multiskan spectrum, Thermo Scientific).

Real-Time Quantitative Polymerase Chain Reaction (qPCR): Osteogenic differentiation of UCB-MSCs was evaluated by examining the expression levels of osteogenic gene markers, alkaline phosphatase (ALP), BSP, Col 1, OCN, OPN, and runt-related transcription factor 2 (RUNX2). Total RNA was isolated from each sample using TRIZOL (Gibco BRL, NY, USA) reagent, followed by determination of the quantity and quality of each RNA sample via a NanoDrop ND-1000 spectrometer (Thermo Scientific, Wilmington, DE). Subsequently, cDNA templates were synthesized using a Maxime RT PreMix kit (Intron, Seoul, Korea) according to the manufacturer's instructions. Upon completion, 1 µL of cDNA from each sample was mixed with Real MOD Green (Intron, Seoul, Korea) and amplified via an ABI 7500 Real-Time PCR system (Applied Biosystems, CA, USA). Gene expression

levels of each sample were analyzed via $2^{-\Delta\Delta CT}$ method. The primers used are as follows: ALP: CCACGTCTTCACATTTGGTG (forward), CAGACTGCGCCTGGTAGTTG (reverse); BSP: CAACCACCCTCTTCACCAC (forward), GATCTTCTGGGGTGGTCTCA (reverse); Col 1: CTGGATGCCATCAAAGTCTTC (forward), AATCCATCGGTCATGCTCTC (reverse); OCN: GGCAGCGAGGTAGTGAAGAG (forward), AGCAGAGCGACACCCTAGAC (reverse);OPN:TGAAACGAGTCAGCTGGATG (forward), TGTGAAAATTCATGGCTGTGG (reverse); RUNX2: TGCACTGGGTCATGTGTTTG (forward), TGGCTGCATTGAAAAGACTG (reverse); and glyceraldehyde-3-phosphate dehydrogenase (GAPDH): GGCTCTCCAGAACATCATCC (forward), TTTCTAGACGGCAGGTCAGG (reverse).[38]

Immunofluorescence Staining (IFS) of Osteogenic Protein Markers: Fixed samples of 14 and 28 d were washed with PBS and treated with peroxo-block solution for 1 min. After blocking, samples were demasked with antigen retrieval reagents for 75 min at 98 °C, permeabilized with 0.1% triton X-100 for 5 min, blocked with 3% BSA for 2 h, and incubated with the primary antibodies – rabbit anti-OCN (Abcam) and goat anti-Col I (Abcam) antibodies diluted in 1% BSA (1:50) – at 4 °C overnight. Samples were then incubated for 1 h at room temperature with corresponding secondary antibodies, Alexa Fluor 488-conjugated goat anti-rabbit IgG (Life Technologies) and Alexa Fluor 594-conjugated donkey anti-goat IgG (Santa Cruz Biotechnology, Inc.), diluted in 1% BSA (1:200). Samples were further subjected to DAPI for nucleic staining of the cells. Fluorescent signals of the target proteins were visualized via confocal microscopy. The positive staining area of each cell was quantified using image processing software (Image J). Three independent samples were examined for each group and fifteen separate regions were imaged for each sample and analyzed using confocal microscope.

Calvarial Bone Defect Model: Rat calvarial defect experiments were conducted in accordance with the institutional guidelines. MCs with or without GFs were encapsulated into collagen scaffolds (8 mm Ø) as previously described; 3 μg of dual GF-loaded MCs were applied per animal. Four experimental groups are G1 (defect only), G2 (3000 ng BMP-2 added in collagen scaffold), G3 (3000 ng BMP-2 delivered from single GF-loaded MCs), and G4 (3000 ng BMP-2/3000 ng VEGF delivered from dual GF-loaded MCs). Total 32 Sprague Dawley rats (SD rats; 7 week-olds; Nara Biotech, Korea) were divided into four groups ($n = 4$, each) for 28D and another four groups ($n = 4$, each) for 56D, respectively. Rats were anesthetized via intraperitoneal injection of Zoletil and Rompun (1 mL kg^{-1}), followed by a sagittal incision over the scalp from the nasal bone to the middle sagittal crest. The periosteum was bluntly dissected and an 8 mm Ø size defect was generated using an automated surgical drilling unit with trephine (Strong 201+Strong 110 LN; Saeshin Precision Co Ltd, Korea), constantly cooled with sterile saline.[39] The calvarial tissues were carefully removed and thoroughly rinsed with saline. The scaffolds were then subsequently implanted in the defect region, after which the periosteum and scalp were sutured using absorbable Vicryl. Rats were monitored daily in the postoperative period for any complications or abnormal behavior. At 28 and 56 d postoperation, the rats were anesthetized as mentioned earlier, placed in a cage with carbon dioxide and euthanized. The transplants were retrieved after atlanto-occipital dislocation and fixed in 10% buffered formalin before further analysis. An incision was made between the medial canthi of the eyes down to the bone using a dissecting scissor. Similarly, cuts were made along the left and right zigmoidal arch and towards the premaxilla arch, resulting in an entire upper region of the cranium containing both defect site and transplant. The brain and skin tissues were excised carefully to minimize tearing of blood vessels within the defect, and specimens were placed in 10% neutral buffered formalin.

Microcomputed Tomography (Micro CT): Micro CT analysis was carried out to quantitatively measure the amount of bone regeneration within the defect. Micro CT images (SkyScan 1172 high-resolution micro CT imaging system; Aartselaar, Belgium) were taken at a resolution of 10 μm with a 0.5 mm aluminum filter, under a voltage of 80 kV and a current of 120 μA. Volumetric reconstruction and analysis was carried out via Nrecon and CT-analyser software of SkyScan with a global threshold of 45–255. The percentage of bone volume in the defect area was calculated using a cylindrical region of interest (ROI) of 8 mm in diameter and 1 mm in height. 3D models of the samples were created as needed using CTVol software provided by Skyscan. Following micro CT scanning, samples were decalcified in 10% ethylenediaminetetraacetic acid (EDTA) at room temperature for four weeks. All samples were dehydrated in a graded series of ethanol (from 70% to 100%), embedded in paraffin, serially sectioned into 10 μm thick sagittal sections, and stored for subsequent osteogenic analysis.

Histology and SEM: Samples were subjected to hematoxylin and eosin (H&E) and von Kossa staining following a standard protocol. Calcium deposits appeared as black or brownish-black spots and images were taken using optical microscopy (Carl Zeiss Axio Vert. A1 Microscope, Germany). Sagittal in vivo sections were dehydrated through a graded series of ethanol (50% to 100%), dried completely, sputter-coated with platinum, and imaged via SEM to analyze the formation of blood vessels within the defect region. Multiple regions within the defect sites were analyzed for the presence of RBCs and used to quantify vessel density (Image J). Quantitative analysis was performed using Image J software (NIH). The H&E-stained sections (two slices per defect, three microscopic fields per ROI) were photographed and used to quantify the mean vessel density, and mean vessel occupied area as assessed by the position of RBCs.

Immunofluorescence Staining of Angiogenic Protein Markers: Angiogenic markers, α-SMA and vWF were assessed. The sagittal in vivo sections were washed, air-dried, and blocked for endogenous peroxidase activity with H_2O_2 diluted in water. After blocking, samples were demasked with antigen retrieval reagents for 75 min at 98 °C, followed by blocking with 3% BSA in PBS for 1 h. The samples were then incubated with mouse monoclonal anti-α-SMA and goat monoclonal anti-vWF diluted in 1% BSA (1:50) at 4°C overnight. Samples were rinsed three times with PBS before the appropriate secondary antibodies; donkey anti-mouse IgG H&L Alexa Fluor 555 and Alexa Fluor 488-conjugated donkey anti-goat IgG, diluted in 1% BSA (1:200), were added to the sample and incubated at room temperature for 1 h. Fluorescence images of the target proteins were observed using a laser scanning confocal microscope (Zeiss LSM 700; Carl Zeiss Micro-Imaging GmbH, Germany). Positive stains of OCN, Col I, α-SMA, and vWF in the fluorescence images were subjected to threshold processing and analyzed using the area measurement tool of image processing software (Image J, NIH).

Statistical Analysis: All data presented were obtained from five (in vitro) or four (in vivo) independent samples, each analyzed in triplicate. A one-way analysis of variance (ANOVA) with Tukey's multiple comparison post hoc test was conducted using a commercial software (GraphPad Prism 5, San Diego, USA). Statistically significant difference was determined as * ($p < 0.05$), ** ($p < 0.01$), and *** ($p < 0.001$), respectively.

Supporting Information

Supporting Information is available from the Wiley Online Library or from the author.

Acknowledgements

[1] A. Khojasteh, H. Behnia, N. Naghdi, M. Esmaeelinejad, Z. Alikhassy, M. Stevens, *Oral Surg. Oral Med. Oral Pathol.* **2013**, *116*, e405.

[2] N. Kimelman, G. Pelled, G. A. Helm, J. Huard, E. M. Schwarz, D. Gazit, *Tissue Eng.* **2007**, *13*, 1135.

[3] Y. Liao, X. L. Zhang, L. Li, F. M. Shen, M. K. Zhong, *Br. J. Clin. Pharmacol.* **2014**, *78*, 718.

[4] K. Lee, E. A. Silva, D. J. Mooney, *J. R. Soc. Interface* **2011**, *8*, 153.

[5] T. P. Richardson, M. C. Peters, A. B. Ennett, D. J. Mooney, *Nat. Biotechnol.* **2001**, *19*, 1029.

[6] D. H. Choi, R. Subbiah, I. H. Kim, D. K. Han, K. Park, *Small* **2013**, *9*, 3468.

[7] H. Park, J. S. Temenoff, Y. Tabata, A. I. Caplan, R. M. Raphael, J. A. Jansen, A. G. Mikos, *J. Biomed. Mater. Res: Part B* **2009**, *88A*, 889.

[8] C. Borselli, H. Storrie, F. Benesch-Lee, D. Shvartsman, C. Cezar, J. W. Lichtman, H. H. Vandenburgh, D. J. Mooney, *Proc. Natl. Acad. Sci. U.S.A.* **2010**, *107*, 3287.

[9] A. Hernández, R. Reyes, E. Sanchez, M. Rodríguez-É vora, A. Delgado, C. Evora, *J. Biomed. Mater. Res. Part A* **2012**, *100A*, 2382.

[10] R. Subbiah, P. Du, M. P. Hwang, I. G. Kim, S. Y. Van, Y. K. Noh, H. Park, K. Park, *Macromol. Res.* **2014**, *22*, 1320.

[11] C. A. Simmons, E. Alsberg, S. Hsiong, W. J. Kim, D. J. Mooney, *Bone* **2004**, *35*, 562.

[12] H. Peng, A. Usas, A. Olshanski, A. M. Ho, B. Gearhart, G. M. Cooper, J. Huard, *J. Bone Miner. Res.* **2005**, *20*, 2017.

[13] J. M. Kanczler, P. J. Ginty, L. White, N. M. Clarke, S. M. Howdle, K. M. Shakesheff, R. O. Oreffo, *Biomaterials* **2010**, *31*, 1242.

[14] M. Samee, S. Kasugai, H. Kondo, K. Ohya, H. Shimokawa, S. Kuroda, *J. Pharmacol. Sci.* **2008**, *108*, 18.

[15] B. De la Riva, E. Sanchez, A. Hernandez, R. Reyes, F. Tamimi, E. Lopez-Cabarcos, A. Delgado, C. Evora, *J. Controlled Release* **2010**, *143*, 45.

[16] S. Young, Z. S. Patel, J. D. Kretlow, M. B. Murphy, P. M. Mountziaris, L. S. Baggett, H. Ueda, Y. Tabata, J. A. Jansen, M. Wong, A. G. Mikos, *Tissue Eng. Part A* **2009**, *15*, 2347.

[17] Z. S. Patel, S. Young, Y. Tabata, J. A. Jansen, M. E. K. Wong, A. G. Mikos, *Bone* **2008**, *43*, 931.

[18] H. I. Canter, I. Vargel, P. Korkusuz, F. Oner, D. B. Gungorduk, B. Cil, E. Karabulut, M. F. Sargon, Y. Erk, *Ann. Plast. Surg.* **2010**, *64*, 342.

[19] D. H. R. Kempen, L. Lu, A. Heijink, T. E. Hefferan, L. B. Creemers, A. Maran, M. J. Yaszemski, W. J. A. Dhert, *Biomaterials* **2009**, *30*, 2816.

[20] F. Danhier, E. Ansorena, J. M. Silva, R. Coco, A. Le Breton, V. Preat, *J. Controlled Release* **2012**, *161*, 505.

[21] R. Poojari, R. Srivastava, *Exp. Opin. Drug Delivery* **2013**, *10*, 1061.

[22] R. Subbiah, M. Veerapandian, K. Yun, *Curr. Med. Chem.* **2010**, *17*, 4559.

[23] T. Maruyama, Y. Fukui, E. Tsuchiya, A. Fujii, *RSC Adv.* **2012**, *2*, 11672.

[24] N. Bock, M. A. Woodruff, D. W. Hutmacher, T. R. Dargaville, *Polymers* **2011**, *3*, 131.

[25] R. Sridhar, S. Ramakrishna, *Biomatter* **2013**, *3*, e24281.

[26] J. M. Kanczler, R. O. C. Oreffo, *Eur. Cell. Mater.* **2008**, *15*, 100.

[27] S. E. Bae, J. S. Son, K. Park, D. K. Han, *J. Controlled Release* **2009**, *133*, 37.

[28] S. Zhang, H. Uludağ, *Pharm. Res.* **2009**, *26*, 1561.

[29] H. Bysell, R. Mansson, P. Hansson, M. Malmsten, *Adv. Drug Delivery Rev.* **2011**, *63*, 1172.

[30] Y. Zhang, V. Madhu, A. S. Dighem, J. N. Irvine, Q. Cui, *Growth Factors* **2012**, *30*, 333.

[31] Y. Q. Yang, Y. Y. Tan, R. Wong, A. Wenden, L. K. Zhang, A. B. Rabie, *Int. J. Oral Sci.* **2012**, *4*, 64.

[32] M. Frohlich, W. L. Grayson, L. Q. Wan, D. Marolt, M. Drobnic, G. Vunjak-Novakovic, *Curr. Stem Cell Res. Ther.* **2008**, *3*, 254.

[33] C. Weinand, A. Nabili, M. Khumar, J. R. Dunn, J. Ramella-Roman, J. C. Jeng, M. H. Jordan, Y. Tabata, *Rejuvenation Res.* **2011**, *14*, 185.

[34] J. S. Gabbay, J. B. Heller, S. A. Mitchell, P. A. Zuk, D. B. Spoon, K. L. Wasson, R. Jarrahy, P. Benhaim, J. P. Bradley, *Ann. Plast. Surg.* **2006**, *57*, 89.

[35] R. Subbiah, P. Du, S. Y. Van, M. Suhaeri, M. P. Hwang, K. Lee, K. Park, *Biomed. Mater.* **2014**, *9*, 065003.

[36] R. Subbiah, S. Ramasundaram, P. Du, K. Hyojin, D. Sung, K. Park, N.-E. Lee, K. Yun, K. J. Choi, *J. R. Soc. Interface* **2013**, *10*, 20130694.

[37] N. Rajan, J. Habermehl, M.-F. Cote, C. J. Doillon, D. Mantovani, *Nat. Protoc.* **2007**, *1*, 2753.

[38] K. J. Livak, T. D. Schmittgen, *Methods* **2001**, *25*, 402.

[39] P. P. Spicer, J. D. Kretlow, S. Young, J. A. Jansen, F. K. Kasper, A. G. Mikos, *Nat. Protoc.* **2012**, *7*, 1918.